Spatial gradient sensing and chemotaxis via excitability in *Dictyostelium discoideum*

Daniel P. Shams
Interdisciplinary Biological Sciences, Northwestern University, Evanston, Illinois 60201, USA

Xingbo Yang
Department of Molecular and Cellular Biology, Harvard University, Cambridge, Massachusetts 02138, USA

Pankaj Mehta
Department of Physics, Boston University, Boston, Massachusetts 02467, USA

David J. Schwab
Initiative for the Theoretical Sciences, The Graduate Center, City University of New York, New York, New York 10016, USA

(Received 8 April 2019; accepted 13 August 2019; published 12 June 2020)

The social amoeba *Dictyostelium discoideum* performs chemotaxis under starvation conditions, aggregating towards clusters of cells following waves of the signaling molecule cAMP. Cells sense extracellular cAMP and produce internal caches of cAMP to be released, relaying the signal. These events lead to traveling waves of cAMP washing over the population of cells. While much research has been performed to understand the functioning of the chemotaxis network in *D. discoideum*, limited work has been done to link the operation of the signal relay network with the chemotaxis network to provide a holistic view of the system. We take inspiration from *D. discoideum* and propose a model that directly links the relaying of a chemical message to the directional sensing of that signal. Utilizing an excitable dynamical systems model that has been previously validated experimentally, we show that it is possible to have both signal amplification and perfect adaptation in a single module. We show that noise plays a vital role in chemotaxing to static gradients, where stochastic tunneling of transient bursts biases the system towards accurate gradient sensing. Moreover, this model also automatically matches its internal time scale of adaptation to the naturally occurring periodicity of the traveling chemical waves generated in the population. Numerical simulations were performed to study the qualitative phenomenology of the system and explore how the system responds to diverse dynamic spatiotemporal stimuli. Finally, we address dynamical instabilities that impede chemotactic ability in a continuum version of the model.

DOI: 10.1103/PhysRevE.101.062410

I. INTRODUCTION

The social amoeba *Dictyostelium discoideum* performs a well orchestrated collective behavior as part of its life cycle. For the majority of its life, *D. discoideum* acts as a single cell that forages for food following lactic acid trails from bacteria. However, under starvation conditions a dramatic change occurs. Groups of cells within the population become emergent aggregation centers, emitting cyclic adenosine monophosphate (cAMP) into the extracellular environment in a synchronized fashion. Other cells sense this extracellular cAMP and respond by producing intracellular cAMP that they extrude into the extracellular environment. Eventually, a large population of cells is pulsing spiral waves of cAMP, synchronized with a global period of 6–10 min determined largely by intracellular dynamics. As the population of cells senses and emits cAMP, the signal to begin aggregation is propagated [1]. Cytoskeletal rearrangements allow for the creation of pseudopodia that propel the cell forward in the direction of the aggregation center. Once reaching the aggregation center, cells begin to form a multicellular fruiting body that can sporulate and reproduce the next generation of cells [2].

To aggregate, cells need to not only relay the signal but also need to perform chemotaxis, moving in response to a chemical gradient [3]. Chemotacting cells must execute multiple tasks, such as gradient sensing, polarization, motility, and signaling (production and relaying of cAMP) to achieve felicitous collective aggregation [4]. While there are a number of models for chemotaxis in *D. discoideum*, no consensus solution yet exists for the mechanisms involved, in contrast to the well understood bacterial chemotaxis. Unlike bacterial chemotaxis fully described in *E. coli*, *D. discoideum* utilizes spatial gradient sensing rather than temporal gradient sensing (sensing a chemical spatially across the cell rather than sensing a chemical at different time points) to bias movement [5–12]. In spatial gradient sensing, the cell computes a concentration difference of cAMP across its cell membrane and biases its direction towards an increasing cAMP concentration.

A central challenge for *D. discoideum* when using spatial gradient sensing to successfully aggregate is known as the "back-of-the-wave" problem. As a wave of cAMP washes over a cell, the direction of the increasing gradient must necessarily reverse. If the cell were to passively follow an increasing gradient, the cell would first move towards the

wave origin as it approaches and then in the opposite direction as the wave washes over the cell. However, this behavior is not observed biologically where cells have persistence in the direction from where the wave originated [13]. The means by which a cell maintains persistence despite the reversed gradient on the back of a cAMP wave has been coined the back-of-the-wave problem [4,8,14].

To successfully rectify these dynamic waves, cells must match the internal time scale of mechanisms responsible for adaptation or desensitization in spatial gradient sensing to the time scale of wave incidence. In populations of *D. discoideum* cells, cAMP oscillations occur on a time scale of 6–10 min [15]. If the spatial gradient sensing network has an adaptation process on the same time scale as cAMP signal relay, then the back-of-the-wave problem could be readily solved. In this regime, the cell would only respond to the incoming wave, when the local gradient is in the same direction as the wave's origin, as the adaptation process would cause the cell to be refractory during the back of the wave. A natural way to have the chemotactic time scale match the wave period is to have the processes of signal relay and gradient sensing be driven by the same network.

The process responsible for the creation of population-scale cAMP oscillations is controlled under the signaling pathway [16]. While much work has been performed to understand the signaling pathways, much is still unknown [15,17,18]. In previous work, the signaling pathway was faithfully modeled using a universality based approach under a noisy FitzHugh-Nagumo (FHN) model [19]. In this model, extracellular cAMP, or intracellular noise, has the ability to excite the system into creating a transient pulse of cAMP exhibited by a spike in the level of an activator molecule. The increase in the activator incites a positive feedback loop while also causing slower accumulation of a repressor, ultimately leading to a pulse of cAMP that is released into the extracellular environment. The FHN model is a classic example of an excitable system that exhibits a bifurcation to relaxation oscillations due to a supercritical Hopf bifurcation [20–22].

In this work, we extend the ideas presented in [19] and study how such an excitable signaling network could also be used to perform spatial gradient sensing in a single module. This work, while inspired by *D. discoideum*, depicts a possible mechanism for spatial gradient sensing via excitability, rather than being intended as a complete and accurate model of *D. discoideum*'s chemotaxis network. This model naturally solves the back-of-the-wave problem, provides amplification of a shallow chemical gradient, and is able to concomitantly exhibit perfect adaptation. We also show that its behavior reproduces previous experimental results on *D. discoideum* and provides experimental predictions.

II. A TWO-COMPARTMENT MODEL FOR SPATIAL GRADIENT SENSING

To begin our analysis, we consider a simple toy model of a *D. discoideum* cell with two compartments denoted "front" and "back." When we apply a gradient in this toy model, we simply mean that the front has a higher signal than the back. The leading edge of the cell is responsible for sensing and pseudopod formation with localized actin activation, while the lagging edge generates an extensive myosin network required for proper chemotaxis [9,23,24]. For the remainder of this work, we will refer to the leading edge of the cell as the front and the lagging edge as the back of the cell.

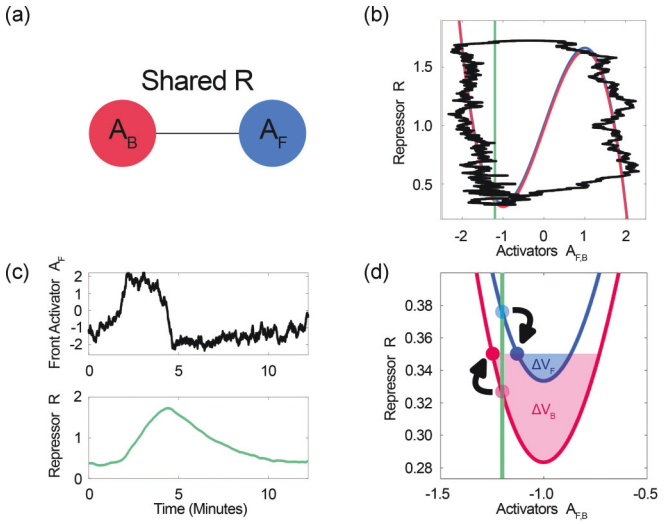

FIG. 1. The two-compartment FHN model. (a) A visual representation of the two-compartment FHN model. Two activators, A_F and A_B exist at the 'front' or the 'back' (leading or lagging edge) of the cell, respectively, with a shared repressor. (b) Phase portrait of the A_F, A_B, and R nullclines (blue, red, and green, respectively) with a single transient burst trajectory of A_F in black. (c) Time course of the the 'front' activator A_F transient burst from (b) and the respective R response caused by internal noise under a static gradient. (d) 2D visualization of the fixed point structure. While the system only has one fixed point, we represent it in a 2D plane to demonstrate how repressor coupling alters the fixed point in A_F and A_B in the presence of a gradient. If the front and back were uncoupled (the fixed points indicated by the opaque dots) the system would require the same amount of energy to activate either compartment. Instead, by sharing a repressor the fixed point moves forward in A_F while also moving backwards in A_B and therefore generates sensitivity to an incoming gradient. The effective potential barriers ΔV_F and ΔV_B described by equation 5 that must be crossed for excitation to a transient burst are visualized in shaded blue and red, respectively. $\sigma = 0.4$ for B and C, $S_F = 1$ and $S_B = 0.97$ for B, C, and D.

We consider the following dimensionless FitzHugh-Nagumo (FHN) system that models the aforementioned two-compartment toy model:

$$\frac{dA_F}{dt} = A_F - \frac{A_F^3}{3} - R + I(S_F) + \eta_F(t), \tag{1}$$

$$\frac{dA_B}{dt} = A_B - \frac{A_B^3}{3} - R + I(S_B) + \eta_B(t), \tag{2}$$

$$\frac{dR}{dt} = \left(\frac{A_F + A_B}{2} + c_0\right)\epsilon. \tag{3}$$

The front and back compartments each have their own activator species, A_F and A_B respectively [Fig. 1(a)]. The repressor R is shared between the compartments and is activated by both A_F and A_B symmetrically. S_F and S_B represent the local level of the extracellular stimulus at the front and back, respectively

(such as cAMP concentration in *D. discoideum*), the function I encodes a preprocessing module acting on the signal $I(x) = a\ln(1 + \frac{x}{K_d})$ where K_d corresponds to the threshold for response of cAMP and a determines the magnitude of the response, c_0 is the steady-state activator value, $\eta_F(t)$ and $\eta_B(t)$ represent Langevin noise satisfying $\langle \eta(t)\eta(t')\rangle = \sigma^2\delta(t-t')$ where σ^2 is the strength of the noise, and $\epsilon = \frac{\tau_A}{\tau_R}$ sets the time-scale ratio of the activators and the repressor ($a = 0.058$, $K_d = 10^{-5}$, and $\epsilon = 0.1$ to mirror experimental results in the signaling relay network [19]). We set $c_0 = 1.2$, keeping the system outside of the oscillatory regime but close enough to allow for transient excitable bursts. In the presence of a stimulus, such as a gradient or noise, the system can become excited to create a single transient burst in either or both compartments, depending on the stimulus, after which the activators fall back to low levels [Figs. 1(b) and 1(c)]. The system is then refractory before returning to the vicinity of the fixed point. Subsequently, a new stimulus must be added to the system for another transient burst to occur. The time scale of these transient bursts is determined by the system's parameters, in particular ϵ, and is similar to the period of the relaxation oscillations that occur in the oscillatory regime [20,25].

The two-compartment FHN system is an extension of the excitable model for the signaling network in *D. discoideum* presented in [19]. The excitable signaling network in [19] requires one activator and repressor to respond if a stimulus is present and generate the phenomenology of the signaling network. However, as we wish to have a system capable of sensing the direction from which a stimulus originates, two compartments each with independent activators and a shared repressor are required. With this two-compartment model, the system not only responds if a stimulus is present, but also responds at the compartment in the directions from where the stimulus originates first. By tuning the speed at which the shared repressor responds after the activator, we generate the phenomenology of spatial gradient sensing.

III. SENSITIVITY WITH PERFECT ADAPTATION AND NOISE-DRIVEN BARRIER CROSSING

We begin our analysis by understating the properties of the two-compartment FHN system with different stimuli. While we ultimately want to apply dynamic gradients to the system, we first apply a simpler static gradient S. By static, we mean that the concentration of S at each compartment does not change in time. We let $S_F > S_B$ so that the gradient is increasing in the direction of the front of the cell, similar to biological cAMP waves generated by *D. discoideum*. In the presence of a static gradient, the system sits at the fixed point and requires energy to be excited.

Noise-driven barrier crossing to excitation has been analyzed in various FHN systems outside of the parameters used in this work [26,27] and has been shown to follow Arrhenius or Kramer escape rate equations of the form $\lambda = Ce^{-\Delta V/\sigma^2}$ where λ is the firing rate of transient bursts, ΔV is a potential barrier, and σ^2 replaces K_BT in the classic Arrhenius equation as noise fluctuations drive excitation when S is static.

We wish to show that our FHN system utilizes barrier crossing to excitation to bias the system towards the front of the cell. We first rewrite the dynamics in terms of an instantaneous potential barrier ΔV to begin our analysis of tunneling behavior. We can rewrite Eqs. (1) and (2) more generally with $A_{F,B}$ replacing A_F and A_B as

$$\frac{dA_{F,B}}{dt} = -\frac{\partial V(A_{F,B}, R, S_{F,B})}{\partial A_{F,B}} + \eta(t), \tag{4}$$

where $V(A_{F,B}, R, S_{F,B}) = -\frac{1}{2}A_{F,B}^2 + \frac{1}{12}A_{F,B}^4 + (R - S_{F,B})A_{F,B}$. On the time scale of escaping the dynamics of the left arm of the $A_{F,B}$ nullclines in a static gradient $S_{F,B}$, R is constant, reducing V to a function of one parameter. V is a two well potential with two local minima and one local maxima ($A_{F,B}^- < A_{F,B}^0 < A_{F,B}^+$) located at the three roots of $-\frac{\partial V(A_{F,B},R)}{\partial A_{F,B}} = 0$ or $R = A_{F,B} - \frac{1}{3}A_{F,B}^3 + S_{F,B}$. We can then define

$$\Delta V_{F,B}(R) = V\left(A_{F,B}^0, R, S_{F,B}\right) - V(A_{F,B}^-, R, S_{F,B}), \tag{5}$$

which provides us with the barrier that blocks transient bursts unless crossed [Fig. 1(d)].

Following Eq. (5), $\Delta V_{F,B}$ is a function of R and $S_{F,B}$. $S_{F,B}$ shifts the A_F nullclines up and the A_B nullcline down in the $A_{F,B}$-R plane [Fig. 1(d)]. As R is shared between A_F and A_B but $S_F > S_B$, then the shape of the potentials V_F and V_B are different. As $S_F > S_B$, then $\Delta V_F < \Delta V_B$ and less energy is necessary to cause an excitation event in A_F than it is in A_B. Simply put, as the fixed point moves towards the bifurcation, $\Delta V \mapsto 0$. Additionally, the system maintains sensitivity in an elevated background stimulus concentration. The roots of V do not change when a background stimulus concentration is present as the difference in static gradient $S_F - S_B$ remains constant and does not change the shape of V.

Using $\Delta V_{F,B}$, we next show that the two-compartment system follows an Arrhenius rate equation $\lambda = Ce^{-\Delta V_{F,B}/\sigma^2}$ to bias the front of the cell to be activated. The ratio of the transient bursting rate of A_F and A_B, $\frac{\lambda_F}{\lambda_B}$, must have a linear relationship to $e^{-(\Delta V_F + \Delta V_B)/\sigma^2}$ for the system to follow the Arrhenius rate equation. For our system, this is exactly what we see [Fig. 2(a)]. While the exact form of the rate equation cannot be solved (due to both excitability and noise being away from idealized limits), our system nonetheless follows Arrhenius-like behavior in a static gradient.

What does this barrier crossing behavior tell us about the system in a static gradient where $S_F > S_B$? When the internal noise is increased, the potential barriers ΔV_F and ΔV_B can be crossed more readily, and therefore the total number of transient bursts increases monotonically as a function of noise strength σ [Fig. 2(b)]. However, as σ increases, the increased strength of driving fluctuations allows both the smaller ΔV_F and the larger ΔV_B to be crossed more easily, and in fact the fraction of forward transient bursts of A_F, $\frac{N_F}{N_F + N_B}$, where $N_{F,B}$ is the number of transient burst in $A_{F,B}$, decreases monotonically [Fig. 2(c)]. In order to maximize sensing in the forward direction, the system must be in a regime where the noise is large enough to create many transient bursts, but small enough so that the fraction of forward transient bursts remains high, in essence balancing a speed-accuracy tradeoff. If the noise strength is very small all transient bursts will be in the front but they will be very rare, while a very large noise strength

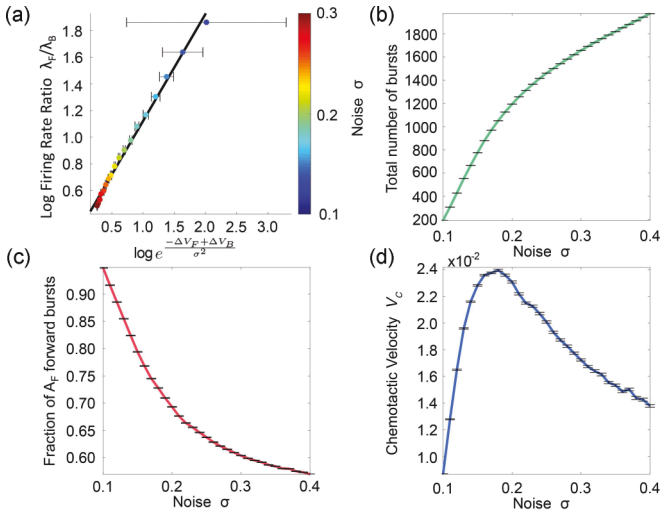

FIG. 2. Barrier crossing and effect of noise on the two-compartment FHN system in a static gradient. (a) A linear relationship exists between the logarithm of the ratio of the firing rate between A_F and A_B and $e^{-(\Delta V_F+\Delta V_B)/\sigma^2}$ following Arrhenius behavior of barrier crossing. The black line represents the line of best fit. Error bars for $\ln(\frac{\lambda_F}{\lambda_B})$ are not shown for clarity as the error is much less than the error in the Arrhenius equation. (b) The total number of transient bursts increases as a function of σ, however (c) the fraction of transients bursts in A_F decreases as a function of σ. (d) The chemotactic velocity (v_C) increases until a certain level of noise σ, whereafter it begins to fall due to the potential barrier ΔV_B being able to be crossed. Error bars represent standard error of the mean (SEM). $S_F = 1$ and $S_B = 0.97$ for all figures.

will cause many transient bursts, but the compartment that bursts will be only slightly biased towards the front.

We define the chemotactic velocity (v_C) as

$$v_C = \frac{N_F - N_B}{T}, \tag{6}$$

where T is total time in minutes. v_C is intended to measure the cell's eventual motility during chemotaxis. We use the word "velocity" to describe Eq. (6) as v_C is a measurement of how much distance a cell could move over time if pseudopodia were created by compartment activation. As spatial gradient sensing is upstream of pseudopod formation, we treat each transient burst as an event that could make a pseudopod and move the cell forward or backwards depending on which compartment is excited. Therefore, v_C is a read-out of actual velocity when considering possible cell movement generated from spatial gradient sensing. We find that an optimal level of noise strength σ exists for a given static gradient to achieve the largest v_C [Fig. 2(d)]. This optimal level of noise provides the greatest number of total transient bursts while minimizing back transient bursts. v_C is of the magnitude of 10^{-2} due to how noise affects the dynamics of the FHN system. If the system were oscillating, one transient burst would occur about every 10 min and v_C would be of order 10^{-1}. However, in the excitable regime noise dictates how often the system creates a transient burst. At low noise levels, very few transient bursts occur but they are always in the forward direction. There may be, e.g., one to two forward transient bursts every 100 min and v_C is of order 10^{-2}. As noise is further increased a greater number of both forward and backwards transient bursts occur. At high levels of noise, there may be, e.g., seven forward transient bursts and six backwards transient bursts and v_C again is of the order 10^{-2}.

Previous models of spatial gradient sensing that employ excitable dynamics, such as LEGI-BEN, have relied on an R nullcline with finite slope and uncoupled compartments to sense a shallow spatial gradient and gain sensitivity and also a LEGI processing unit to provide gradient sensitivity and perfect adaptation [11,28,29]. With a finite sloped R nullcline, the fixed points of the system move closer to the bifurcation as the local stimulus concentration increases. With the fixed points closer to their respective bifurcations, the system requires less input to be excited to a transient burst (as ΔV is smaller) and is therefore more sensitive to a gradient.

Unlike previous models, we utilize a FHN system with an infinite sloped R nullcline and a shared repressor. With an infinite sloped R nullcline and without a shared repressor, the system would have two fixed points [Fig. 1(d), faded dots] and would require the same input for either compartment to be excited. However, with a shared repressor, the single fixed point of the system creates sensitivity by being more positive in A_F than A_B [Fig. 1(d), shaded dots]. Therefore, the magnitude of the stimulus required to cause excitation in the front is less than the back, and sensitivity to a stimulus is generated with a shared repressor and a infinite sloped R nullcline. Notably, we also achieve perfect adaptation due to the infinite slope of the R nullcline. The two-compartment FHN system falls back to near basal levels of A_F and A_B before another excitation occurs, which resembles experiments as spatial gradient components display near-perfect adaption [30,31]. Perfect adaptation also makes it so the system can detect small stimulus changes in a background concentration of chemoattractant and is unlikely to oscillate under biologically relevant stimuli. In *D. discoideum* sensitivity to small changes in cAMP occurs in elevated background levels of cAMP as with no background concentration [32]. In background stimulus concentrations, the system maintains the same fixed point in the dimensions of $A_{F,B}$ and only changes in R and therefore maintains sensitivity in background stimulus concentrations. Also, under biologically relevant stimuli, the fixed point of the system will lie on the left branch of the $A_{F,B}$ nullclines and therefore will never move past the bifurcation to oscillations. Under conditions where the stimulus is very large at the front of the cell and very small at the back of the cell, the system can conceivably be pushed into oscillations due to the repressor coupling.

IV. WAVE RECTIFICATION

We have discussed how, in our model, noise driven barrier crossing is responsible for sensing in a static gradient. However, chemotaxis in *D. discoideum* requires the sensing of dynamic spatiotemporal stimuli to achieve felicitous aggregation. With the velocity of cAMP waves produced by *D. discoideum* being $\frac{850\mu m}{7min}$ and the average length of a chemotactic cell being 15 μm the back of the cell experiences the same concentration of cAMP as the front of the cell after approximately 7 s. Therefore, the spatial gradient sensing

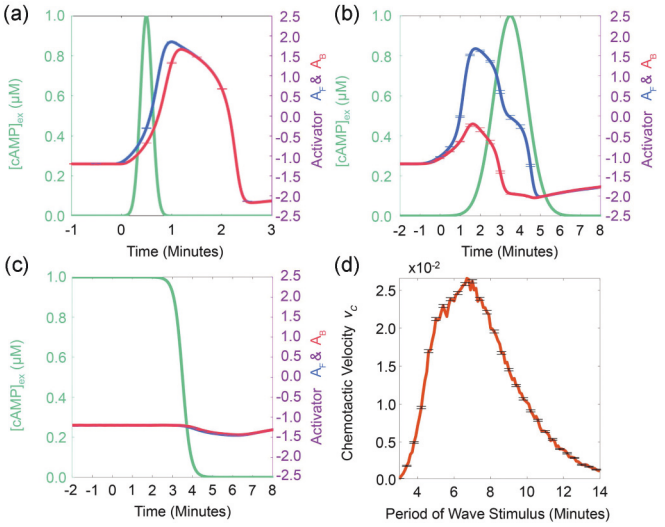

FIG. 3. Wave rectification mirrors biological experiments in the two-compartment FHN model. Simulations of the two-compartment FHN system with varying spatiotemporal stimuli S. (a) A wave of cAMP with a velocity of $\frac{850\ \mu m}{min}$, (b) a wave of cAMP with a velocity of $\frac{850\ \mu m}{7\ min}$ similar to naturally occurring cAMP waves in *Dictyostelim* populations, and (c) a temporally decreasing gradient. The phenomenology seen here mirrors the results from [11]. Time 0 denotes when the stimulus is 0.01% of the maximum concentration and the wave stimulus shown is S_F (S_B not shown for clarity). (d) The stimulus S modeled as an array of Gaussian functions with varying periods (from peak to peak) with a constant velocity of $\frac{850\ \mu m}{7\ min}$. The system provides the best performance when the period of the wave is close to the natural oscillating frequency of the signaling network. Error bars represent standard error of the mean (SEM). $\sigma = 0.035$ for all figures.

machinery must work quickly to repress the back of the cell within this time frame.

D. discoideum produces waves of cAMP with a period of 6–10 min depending on the stage of chemotaxis, shortening as aggregation develops [33]. Previous experiments have shown that the cell's ability to sense a chemoattractant depends greatly on the temporal dynamics of the chemoattractant-containing stimulus, such as the wave of cAMP utilized by *D. discoideum* [11]. If a wave is too fast, the cell senses the wave at both the front and the back of the cell, leading to no net movement. However if the wave is of a biologically relevant period, such as 7 min, the front of the cell senses the wave as it approaches, but the back does not as the wave washes over the cell. To ensure that our model faithfully rectifies spatial gradients, we simulate previously performed experiments analyzing the effect of varying spatiotemporal cAMP waves on the *D. discoideum* spatial gradient sensing component Ras [11].

We first consider a single period of a wave at varying velocities [Figs. 3(a) and 3(b)]. We model the wave as a Gaussian function as this closely mirrors the profile of cAMP waves produced by *D. discoideum* under starvation conditions [34]. Similar to experimental results in *Dictyostelium*, our system has a natural oscillating frequency that allows for dimensionless time T to be converted into dimensionful time for comparison. With dimensionful time, we model the front and the back of the cell by a time difference as to when the stimulus is introduced. The average chemotaxing *Dictyostelium* cell is 15 μm and so providing a wave with a specific velocity allows for the determination of the time lag that the back of the cell experiences a stimulus after the front of the cell [35]. Quick waves ($\frac{850\ \mu m}{min}$) caused transient bursts in both groups of activators A_F and A_B, which is as expected as the shared repressor R doesn't have sufficient time to build up and inhibit activity of A_B [Fig. 3(a)]. Waves of a biologically relevant speed ($\frac{850\ \mu m}{7\ min}$) allow for a time scale where the shared repressor R can inhibit the activator A_B after initial activation of A_F leading to a transient burst [Fig. 3(b)]. As only the front of the cell bursts on a wave of a biologically relevant speed, we show that the model faithfully replicates experimental findings of spatial gradient sensing proteins [11].

Another feature of our two-compartment FHN spatial gradient sensing model is that no transient bursts occur in a temporally decreasing gradient, such as the back of a wave, following experimental results [Fig. 3(c)]. The lack of bursting in a decreasing gradient is due to adaptation, which provides a simple resolution to the back-of-the-wave problem. An input of energy such as S or noise is needed to create a transient burst as outlined in the previous section. In a decreasing gradient, the system begins with a large stimulus present causing $\Delta V_{F,B}$ to be very large. A large amount of energy would be needed to be put into the system to cross $\Delta V_{F,B}$ and create a transient burst. Under the conditions that we use in a decreasing gradient, the level of noise and a decreasing S are unable to cause excitation. Therefore, the back-of-the-wave problem is more accurately described as the top-of-the-wave problem. We use the term top of the wave as the back of the cell must be in an increasing gradient while the front of the cell is in a decreasing gradient for backwards movement to occur with a stimulus that is biologically relevant.

We now consider a continuous wave at a constant velocity ($\frac{850\ \mu m}{7\ min}$) with varying periods. During aggregation, the period of cAMP waves generated by a population of *D. discoideum* varies from 6 to 10 min, with optimal aggregation occurring when the period of the wave is 7 min [11,16,33]. As the adaptation time scale of the signaling network is utilized in our spatial gradient sensing model, optimal gradient sensing naturally occurs when a traveling wave of cAMP with a period of about 7 min is applied to the system as possible excitation is in phase with every incoming wave front [Fig. 3(d)]. The matching of adaptation processes eliminates a need for complex mechanisms to match the adaptation time scales of cAMP production to spatial gradient sensing machinery.

V. CHEMOTAXIS FROM EXCITABLE REACTION-DIFFUSION SYSTEM

While the simplified FHN model presented above captures the qualitative phenomenology of spatial gradient sensing, to model chemotaxis of *D. discoideum*, we need to account for the potential diffusive dynamics of the activator and the repressor across the cell membrane. We next develop a continuum version of the proposed system that lives around a circular cell membrane. Just as in the two-compartment model, if R is not shared, then activation can occur along multiple locations on the cell membrane which will disrupt the

ability to sense a spatial gradient. However, when a globally shared repressor is used in a continuum model, dynamical instabilities are generated. Therefore, the continuum system must have a locally diffusible repressor R with a finite diffusion constant D_R, that should be as large as possible without inducing an instability. In that case, R has the ability to share information across the cell without causing instabilities. As D_R increases, so should the ability to sense a spatial gradient accurately as the system will become blocked from excitation in other locations of the cell membrane more rapidly.

We expand our model into a one-dimensional excitable reaction-diffusion system on the cell membrane to detect spatial gradients [20]. We treat the cell as a flat circular disk with a diffusible activator A and repressor R along the circumference of the disk obeying the dimensionless equations

$$\frac{\partial A(\theta,t)}{\partial t} = A(\theta,t) - (A(\theta,t))^3 - R(\theta,t) + S(\theta) + \nabla^2 A(\theta,t) + \eta(\theta,t), \tag{7}$$

$$\frac{\partial R(\theta,t)}{\partial t} = (A(\theta,t) + c_0)\epsilon + D\nabla^2 R(\theta,t), \tag{8}$$

where $D = \frac{D_R}{D_A}$, D_R and D_A are the diffusion constants of R and A respectively, $S = \cos(\theta)$, and $\eta(\theta,t)$ is Langevin noise decorrelated in space and time satisfying the relation $\langle \eta(\theta,t)\eta(\theta',t')\rangle = \sigma^2\delta(\theta-\theta')\delta(t-t')$. Below we study how diffusion and noise influence chemotaxis via pattern formation in this excitable reaction-diffusion system.

We begin our analysis with $D_R < D_A$ or $D < 1$. In this regime, traveling waves of A are generated [Fig. 4(a), top panel]. These wave solutions are known to exist in the reaction-diffusion FHN system and are well described [36,37]. As the activator A is diffusing more rapidly than the repressor R, the repressor R cannot catch up to the activator A. When $D > 1$, the activator can now be repressed by R as $D_R > D_A$ and transient patches are generated [Fig. 4(a), middle panel] [36]. These patches resemble many signaling components in *D. discoideum* such as Ras and even downstream proteins involved in pseudopod formation such as actin [38].

However, when D is increased further ($D > 10$), stationary pattern states emerge [Fig. 4(a), bottom panel]. When performing linear stability analysis, the system is linearly stable in the absence of noise. Therefore, these pattern states may be transiently generated by noise and we wish to determine the effects of noise on pattern formation and its consequence on chemotaxis in the reaction-diffusion system with large D. As the stationary pattern state exists in the absence of a stimulus, we set $S = 0$ in the following analysis unless otherwise noted. We follow Butler and Goldenfeld's analysis on noise induced pattern formation [39]. If noise has the ability to decay some perturbations slower than others, transient patterns can occur. To begin, we Fourier transform perturbations of the system about the homogeneous steady state solution in both the spatial and temporal domains,

$$(\delta A(\theta,t), \delta R(\theta,t), \eta(\theta,t)) = \iint (A(k,\omega), R(k,\omega), \eta(k,\omega)) e^{i(k\theta-\omega t)} dk d\omega, \tag{9}$$

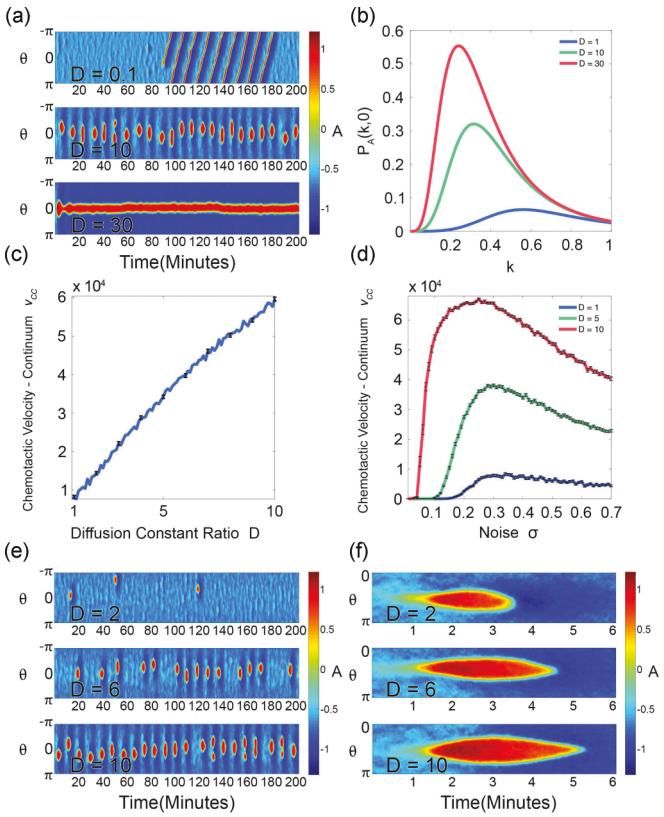

FIG. 4. Effect of noise and the diffusion constant ratio on chemotaxis. The reaction-diffusion FHN models the activity of A and R along the membrane of a disk shaped cell over time. S is modeled as $0.1\cos(\theta)$ in (a) and (c)–(f). (a) Altering D causes phase transitions in the continuum FHN system. For small $D < 1$, traveling waves occur. As D increases past 1, transient patches excited by noise are dynamically generated. However, at $D > 10$ a stochastic stationary pattern state is obtained. (b) As D increases, the peak of the activator power spectrum $P_A(k,0)$ is amplified, depicting noise driven stationary pattern formation. (c) V_{CC} increases roughly linearly as a function of D in the transient patch regime. (d) Just as in Fig. 2(b), noise biases the chemotactic velocity towards the direction of the gradient until a certain point where noise allows for other compartments to burst. As D increases, so does the chemotactic velocity, until $D > 10$ where the stationary pattern state forms. (e),(f) As D is increased so does the rate (e) and the duration (f) of transient bursts. A single representative patch is shown in (f). $\sigma = 0.4$ and $c_0 = 0.62$ for all figures except (d) where noise varies. Error bars represent standard error of the mean (SEM).

substituting in Eqs. (7) and (8), we obtain

$$-i\omega\mathbf{x} = \mathbf{J}\mathbf{x} + \boldsymbol{\eta}, \tag{10}$$

where

$$\mathbf{x} = \begin{bmatrix} A(k,\omega) \\ R(k,\omega) \end{bmatrix}, \quad \mathbf{J} = \begin{bmatrix} 1 - 3c_0^2 - k^2 & -1 \\ \epsilon & -Dk^2 \end{bmatrix},$$

$$\text{and} \quad \boldsymbol{\eta} = \begin{bmatrix} \eta(k,\omega) \\ 0 \end{bmatrix}. \tag{11}$$

We solve for the activator concentration,

$$A(k,\omega) = \frac{Dk^2\eta - i\omega\eta}{\det(J) - \omega^2 + i\omega \mathrm{Tr}(J)}, \tag{12}$$

from which we solve for the power spectrum of A,

$$\begin{aligned} P_A(k,\omega) &= \langle A(k,\omega)A(k,-\omega)\rangle_\eta \\ &= \left\langle \frac{[(-Dk^2)^2+\omega^2]\eta^2}{[\det(J)-\omega^2]^2 + [\omega \mathrm{Tr}(J)]^2} \right\rangle_\eta, \end{aligned} \tag{13}$$

where $\langle \dots \rangle_\eta$ is the average over noise η. With uncorrelated Gaussian noise, $\langle |\eta|^2 \rangle_\eta = \sigma^2$, reducing Eq. (13) to

$$P_A(k,\omega) = \frac{[(-Dk^2)^2+\omega^2]\sigma^2}{[\det(J)-\omega^2]^2 + [\omega \mathrm{Tr}(J)]^2}. \tag{14}$$

Explicitly this is

$$P_A(k,\omega) = \frac{(D^2k^4+\omega^2)\sigma^2}{\left[Dk^2\left(-1+3c_0^2+k^2\right)+\epsilon\right]^2 + \left[\omega\left(1-3c_0^2-k^2-Dk^2\right)^2\right]}. \tag{15}$$

Stationary pattern formation occurs when there is a peak in P_A for $\omega = 0$. From Eq. (15), we see that if $D = 0$ or $\sigma = 0$, no peak exists implying no pattern states exist. However, while σ and D are finite, a peak is introduced and stationary patterns are enhanced by increasing D [Fig. 4(b)].

While increasing D and noise strength σ are beneficial for optimal performance in a static gradient, the presence of noise induced pattern states are detrimental. Biologically, the stationary pattern state represents constant activation along the leading edge of the cell. Activation of spatial gradient sensing proteins along the cell membrane is upstream and required for pseudopod formation, while repression of activated spatial gradient sensing proteins, such as cytosolic regulator of adenylyl cyclase (CRAC), is required for pseudopod retraction [40]. Therefore, if a segment of the cell membrane is constantly activated a pseudopod could be formed, but would never retract and thus no forward movement would occur. On the other hand, if D is too small, traveling wave pattern states would cause the cell to move in circles, thus not making any net movement. Therefore, the interplay between noise and the diffusion constant ratio D is critical in accurate gradient sensing. D can neither be too small (leading to traveling waves) nor too large (leading to stationary patterns), but rather the cell must tune D to an intermediate regime so that transient patches are generated. Interestingly, both stationary pattern formations and traveling waves have been seen in the cell surface proteins of chemotaxing *D. discoideum* [36,40–42], which may be in part caused by the phenomena described above.

While all three states generated by the continuum model are seen in biology, we wish to analyze the most biologically relevant state and focus on the transient patch state ($1 < D \leqslant 10$). To quantify chemotaxis in the presence of a static spatial gradient in the continuum model, we define an analog to v_C called the continuum chemotactic velocity or V_{CC} defined as

$$V_{\mathrm{CC}} = \sum_\theta \sum_t \frac{H(A(\theta,t))\cos(\theta)}{T}, \tag{16}$$

where $H(A)$ is the Heaviside function of the activator A and T is the total time in minutes. Therefore, if a patch occurs at $\theta = 0$, the system will be providing the best performance and the worst performance occurs when a transient burst is at $\theta = \pm\pi$.

As stated earlier, V_{CC} should increase as a function of D in the presence of the static gradient S. Holding noise strength $\sigma = 0.4$ constant, this is indeed the case [Fig. 4(c)]. V_{CC} increases roughly linearly with respect to D. As the signal S has the largest concentration at $\theta = 0$, patches will be biased along this axis [Fig. 4(d)]. However, it is possible for noise to cause excitation in other compartments. Increasing D ensures that after a patch is generated, noisy patches generated at locations where S is low are either short-lived or will not occur as the compartments will already be inhibited. Along with decreasing the chance for noise-driven excitation of compartments along low concentrations of the signal S, increasing D also increases the duration and frequency of transient patches [Figs. 4(e) and 4(f)]. We notice that as $D \mapsto 10$ the characteristic duration of the patches increases. The system appears to be attempting to reach the stationary pattern state, but fails to do so. Therefore, even though the stationary pattern state is not present, increasing D changes the characteristics of the transient patches to be closer to the shape of the stationary pattern state. More so, the rate at which transient patch formation occurs increases as the system is moving closer to the stationary pattern state where activation never becomes repressed. Therefore, the system tends to be constantly activated and the frequency of transient patches increases. This behavior may be due to the size of the basin of attraction for the stationary pattern state being small and therefore difficult for solutions to converge until $D > 10$.

VI. CONCLUSIONS

The system we present here provides a simple solution to time-scale matching between gradient sensing and the signaling network, while providing sensitivity, perfect adaptation, and accurate wave rectification. Utilizing perfect adaptation, we achieve sensitivity and the ability to detect shallow gradient stimuli. Noise provides the necessary energy to push the system past a potential barrier, biasing the sensing of a static spatial gradient towards the origin of that spatial gradient. Expanding our model from a simplified two-compartment model into a one dimensional reaction-diffusion model that lives on the cell membrane, we find that noise interacts with the diffusion constant ratio D to create pattern states that have been seen experimentally and could influence chemotaxis of *Dictyostelium discoideum*.

Allowing the signaling machinery to activate spatial gradient sensing solves one of the major issues in *D. discoideum* chemotaxis. We naturally solve the back-of-the-wave problem as the back of the excitable system will not burst in a decreasing gradient and will not burst in a biologically relevant wave back due to the time scale of adaptation. In hand, we naturally solve the issue of time-scale matching between the signaling network and spatial gradient sensing. In *D. discoideum* starvation-induced chemotaxis, cAMP is released into the extracellular environment every 6-10 min. The ability to sense a spatial gradient of cAMP occurs optimally when the spatial

gradient has a period of 5–9 min. By utilizing the signaling network to perform spatial gradient, we solve this problem by matching their time scales of adaptation automatically.

Having answered these issues with our theory that explains previous experimental findings, we also provide experimental predictions to determine if this theory could be an accurate model for Eukaryotic chemotaxis. Both the two-compartment and the continuum model predict the existence of an optimal chemotactic velocity as a function of noise due to the competition of total bursting rate and bursting fraction of the leading edge. The continuum model predicts a bursting regime at intermediate diffusivity ratio D of repressor and activator, where chemotactic velocity increases with D. At small and large D, traveling wave and stationary pattern states emerge, respectively, due to the interplay of excitability and noise, which could potentially reduce chemotatic capability of the cell. While components of the spatial gradient sensing network in *D. discoideum* are unknown, one component that may be of interest for experimental observation is surface cAMP receptor 1 (cAR 1). cAR1 is the main transmembrane cell surface receptor responsible for sensing cAMP during starvation induced chemotaxis and is upregulated tenfold during aggregation [43,44]. cAR1 is essential to chemotaxis as cells without cAR1 lack the ability to perform any aspects of chemotaxis and cAR1 pathways can display adaptation to cAMP [24,45]. Thus cAR1 may be used as an activational receptor for both the signaling and spatial gradient networks. Subcellular localization and activation of many components in chemotaxis is common in *D. discoideum* and thus localization and activation of cAR1 would not be out of place [44]. While localization assays have been developed for the cAR1 *G*-coupled proteins, a direct assay to determine the activation of cAR1 spatially has yet to be developed [46].

ACKNOWLEDGMENTS

D.P.S. was supported by NIH K25 Grant No. GM098875-02 and D.J.S. was supported as a Simons Investigator in the MMLS, by NIH K25 Grant No. GM098875-02, support from the National Science Foundation through the Center for the Physics of Biological Function (Grant No. PHY-1734030). Thanks to Y. Chen of the Engineering Sciences and Applied Mathematics Department at Northwestern University for providing code for performing linear stability analysis.

[1] M. Postma, J. Roelofs, J. Goedhart, H. M. Loovers, A. J. Visser, and P. J. Van Haastert, J. Cell Sci. **117**, 2925 (2004).
[2] C. Anjard and W. F. Loomis, Development **135**, 819 (2008).
[3] M. Ueda, Y. Sako, T. Tanaka, P. Devreotes, and T. Yanagida, Science **294**, 864 (2001).
[4] M. Skoge, H. Yue, M. Erickstad, A. Bae, H. Levine, A. Groisman, W. F. Loomis, and W.-J. Rappel, Proc. Natl. Acad. Sci. USA **111**, 14448 (2014).
[5] R. A. Arkowitz, Trends Cell Biol. **9**, 20 (1999).
[6] H. C. Berg and E. M. Purcell, Biophys. J. **20**, 193 (1977).
[7] S. Bhattacharya and P. A. Iglesias, *Chemotaxis* (Springer, 2016), pp. 397–415.
[8] A. Bhowmik, W.-J. Rappel, and H. Levine, Phys. Biol. **13**, 016002 (2016).
[9] Y. Cheng and H. Othmer, PLoS Comput. Biol. **12**, e1004900 (2016).
[10] P. A. Iglesias and P. N. Devreotes, Curr. Opin. Cell Biol. **20**, 35 (2008).
[11] A. Nakajima, S. Ishihara, D. Imoto, and S. Sawai, Nat. Commun. **5**, 5367 (2014).
[12] M. Nishikawa, M. Hörning, M. Ueda, and T. Shibata, Biophys. J. **106**, 723 (2014).
[13] D. M. Veltman and P. J. van Haastert, J. Cell Sci. **121**, 120 (2008).
[14] C.-H. Huang and P. A. Iglesias, Proc. Natl. Acad. Sci. USA **111**, 15287 (2014).
[15] K. Tomchik and P. N. Devreotes, Science **212**, 443 (1981).
[16] S. Sawai, P. A. Thomason, and E. C. Cox, Nature (London) **433**, 323 (2005).
[17] F. Alcantara and M. Monk, Microbiology **85**, 321 (1974).
[18] J. J. Tyson, K. A. Alexander, V. S. Manoranjan, and J. D. Murray, Physica D **34**, 193 (1989).
[19] A. E. Sgro, D. J. Schwab, J. Noorbakhsh, T. Mestler, P. Mehta, and T. Gregor, Mol. Syst. Biol. **11**, 779 (2015).
[20] M. Cross and H. Greenside, *Pattern Formation and Dynamics in Nonequilibrium Systems* (Cambridge University Press, Cambridge, UK, 2009).
[21] S. H. Strogatz, *Nonlinear Dynamics and Chaos: With Applications to Physics, Biology, Chemistry, and Engineering* (Westview, Reading, MA, 2014).
[22] B. Van der Pol, Radio Rev. **1**, 701 (1920).
[23] A. Kortholt, I. Keizer-Gunnink, R. Kataria, and P. J. Van Haastert, J. Cell Sci. **126**, 4502 (2013).
[24] A. R. Kimmel and R. A. Firtel, Curr. Opin. Genet. Dev. **14**, 540 (2004).
[25] S. M. Baer and T. Erneux, SIAM J. Appl. Math. **46**, 721 (1986).
[26] B. N. Lundstrom, M. Famulare, L. B. Sorensen, W. J. Spain, and A. L. Fairhall, J. Comput. Neurosci. **27**, 277 (2009).
[27] R. E. L. DeVille, E. Vanden-Eijnden, and C. B. Muratov, Phys. Rev. E **72**, 031105 (2005).
[28] P. N. Devreotes, S. Bhattacharya, M. Edwards, P. A. Iglesias, T. Lampert, and Y. Miao, Annu. Rev. Cell Dev. Biol. **33**, 103 (2017).
[29] M. Tang, M. Wang, C. Shi, P. A. Iglesias, P. N. Devreotes, and C.-H. Huang, Nat. Commun. **5**, 5175 (2014).
[30] J. E. Ferrell, Jr., Cell Syst. **2**, 62 (2016).
[31] H. Levine, W.-J. Rappel, and I. Cohen, Phys. Rev. E **63**, 017101 (2000).
[32] L. Ma, C. Janetopoulos, L. Yang, P. N. Devreotes, and P. A. Iglesias, Biophys. J. **87**, 3764 (2004).
[33] T. Gregor, K. Fujimoto, N. Masaki, and S. Sawai, Science **328**, 1021 (2010).
[34] P. N. Devreotes, M. J. Potel, and S. A. MacKay, Dev. Biol. **96**, 405 (1983).

[35] B. Varnum and D. R. Soll, J. Cell Biol. **99**, 1151 (1984).
[36] I. Hecht, D. A. Kessler, and H. Levine, Phys. Rev. Lett. **104**, 158301 (2010).
[37] H. Henry and H. Levine, Phys. Rev. E **68**, 031914 (2003).
[38] Y. Artemenko, T. J. Lampert, and P. N. Devreotes, Cell. Mol. Life Sci. **71**, 3711 (2014).
[39] T. Butler and N. Goldenfeld, Phys. Rev. E **80**, 030902(R) (2009).
[40] M. Postma, J. Roelofs, J. Goedhart, T. W. Gadella, A. J. Visser, and P. J. Van Haastert, Mol. Biol. Cell **14**, 5019 (2003).
[41] M. G. Vicker, Exp. Cell Res. **275**, 54 (2002).
[42] G. Gerisch, T. Bretschneider, A. Müller-Taubenberger, E. Simmeth, M. Ecke, S. Diez, and K. Anderson, Biophys. J. **87**, 3493 (2004).
[43] M. J. Caterina, J. Milne, and P. N. Devreotes, J. Biol. Chem. **269**, 1523 (1994).
[44] V. C. McMains, X.-H. Liao, and A. R. Kimmel, Ageing Res. Rev. **7**, 234 (2008).
[45] P. S. Klein, T. J. Sun, C. L. Saxe, A. R. Kimmel, R. L. Johnson, and P. N. Devreotes, Science **241**, 1467 (1988).
[46] C. Janetopoulos, T. Jin, and P. Devreotes, Science **291**, 2408 (2001).